Dielectrophoresis can control the density of CNT membranes as confirmed by Experiment and Dissipative Particle Simulation

Canh-Dung Tran[1,*], Khoa Le-Cao[2], Bui Thanh Tung[3], Van Thanh Dau[4]

[1] School of Mechanical and Electrical Engineering, University of Southern Queensland,

[2]Department of Mechanical Engineering, National University of Singapore,

[3]Faculty of Electronic Engineering, Hanoi University of Industry,

[4] School of Engineering and Built Environment, Griffith University,

Abstract: In forests and membranes, Carbon nano tubes (CNT) are not individual, instead they tend to be agglomerated into bundles because of the strong van der Waals interaction. CNTs usually form into bundles containing up to hundreds or thousands of parallel CNTs named as fibres which create networks within a CNT membrane. Recently, CNT based macrostructures (yarn and membrane) have increasingly been used in various applications in electronics, medical and bioengineering. Meanwhile the volume density of CNTs impacts on mechanical and physical properties of macrostructures, the controlling of the density of membranes is very complex. Thus, in this paper, an electric processing to dilate CNT membrane is sufficiently studied and investigated by both the experiment and particle based numerical simulation. Several initially potential applications of the method are also represented not only to control the density of CNTs but also to improve the CNTs' alignment in macro-structures.

1. Introduction

The CNT macrostructures including yarns and membranes start by forming web, whereby a forest of vertically oriented CNTs is converted to a horizontally continuous web [1]–[4] (Fig.1a). CNT fibres are oriented along the web axis in a variety of ways, some of them are parallel and others are poorly aligned or coiled [1]–[4] (Fig.1b). Since the CNT web impacts on the properties of derived macrostructures, the simulation of CNT membranes has attracted significant attentions [4]–[6]. For example, a model by Kunznetsov and his co-workers [4] proposed that the connection between CNT fibres is the basis for the continuous spinning of CNT web and then yarn from CNT forests. Such models postulate that the densification effect at the top and bottom of the forest strengthens the fibres interconnections when being pulled out a CNT wafer. However, the scanning electron microscopy (SEM) analysis of CNT webs showed that CNT fibres entangle together (Fig. 1.b). This entanglement is a key factor for the formation of CNT macrostructures because it allows the array of parallel fibres to unfold continuously into a CNT networks. In other words, the entanglement of CNT fibres can be

*Corresponding author. Tel: 61.07.46875804. Email: Canh-Dung.Tran@usq.edu.au (Canh-Dung Tran)

regarded as networks made of fibres' entanglement junctions (Fig. 2) [2], which have a strong relationship with the properties of derived CNT macrostructures. We reckon that CNT fibres are movable because the constraint imposed by the surrounding CNTs can change due to their own motion and a constraint will disappear if the surrounding CNTs shift. Thus, the entanglement of CNTs within a membrane (or fibre) can be modelled using the dual slip-link theory which was introduced by Doi and Takimoto [7] in modelling polymeric materials. For this model, the entanglement junction is represented by a slip link through which fibres can pass freely. The CNT fibres are linked together by slip links, which can be destroyed if fibres slide off the slip links. This model corresponds to the formation of a random network of CNT fibres with non-uniform tension pulled out of a CNT forest. Owing to such structure, CNT membrane can be flexible by a load. Over the last two decades, CNT membrane has increasingly been used in various applications of electronics, medical and bioengineering [9],[10]. While the density of CNTs impacts on mechanical and physical properties of CNT membranes, the processing of CNT membrane density is interesting but very challenging.

Besides aligning CNTs in macrostructures using electric field as stated in [10]–[14], a phenomenon in which a force exerted on a dielectric particle when it is subjected to an electric field (named as the dielectrophoresis [15]) is considered in this work. This force strongly depends on the medium and particle electrical properties, the particle's shape and size, as well as the frequency of the electric field. The present method based on this principle is developed for the separation of CNT fibres from each other to control the density/porosity of CNT membranes. Both experiment and Dissipative particle dynamics (DPD) based numerical method have been successfully investigated and evaluated for a range of electric fields using the alternative current (AC) of different applied voltages and frequencies.

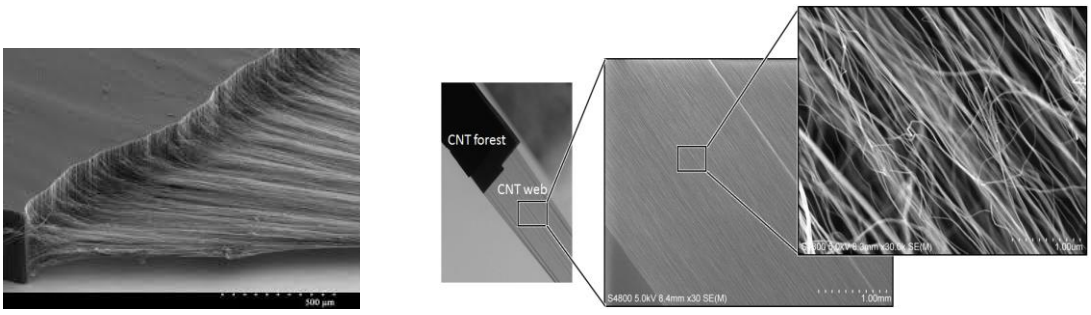

(a) (b)

Figure 1. Dry spinning method of CNTs: (a) CNT membrane pulled out from a CNT forest; and (b) A structure of CNT web observed by SEM

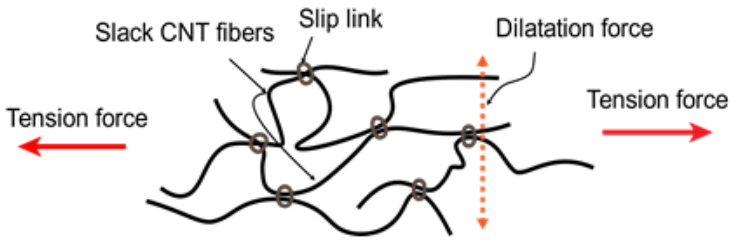

Figure 2. Dual slip-link theory based model of CNT membrane

2. Dilating CNT membrane using the dielectrophoresis

2.1. Review on the interaction energy between CNT fibres

In macro-structures such as fibres, yarns and membranes, CNTs tend to agglomerate in the form of entangled and close-packed bundles. The interaction energy of two CNTs can be approximated by summing up the interaction between pairs of carbon atom Φ, using the Lennard Jones potential as follows [16], [17].

$$\phi(d) = 4\varepsilon\left[\left(\frac{\sigma}{d}\right)^{12} - \left(\frac{\sigma}{d}\right)^{6}\right], \tag{1}$$

where d is the distance between atomic centres; ε the depth of the potential energy well; σ the spacing where the potential energy is zero. Details of these parameters can be found in [18,19].

The potential energy between several two nano-structures, for example, CNT-CNT, CNT-ropes, graphene-graphene can be determined by integrating the Lennard–Jones potential over the surface of the structure using the generalized potential function [17].

$$\phi(\bar{d}) = -\frac{|\phi(d_0)|}{0.6}\left(\left(\frac{3.41}{3.13\bar{d}+0.28}\right)^{4} - 0.4\left(\frac{3.41}{3.13\bar{d}+0.28}\right)^{10}\right) \tag{2}$$

where d, d_o and ρ are the centre to centre spacing of the CNTs, the equilibrium distance (the distance between CNT centres at the unloaded state) and the distance characteristic of the specific geometries in the interaction, respectively; $|\phi(d_0)|$ the energy well depth and $\bar{d}$ is the normalized distance and given as follows

$$\bar{d} = \frac{d-\rho}{d_0-\rho} \tag{3}$$

Parameters d_o, ρ and $|\phi(d_0)|$ depend on the chiral pair of CNTs and are given in Table 1.

Table 1: Universal potential function parameters of some chiral pairs of CNTs [17]

System	Energy well depth $\lvert\Phi(d_0)\rvert$ (nJ/m)	Equilibrium spacing d_0 (nm)	Distance parameter ρ (nm)
(6,6) – (6,6) CNTs	0.1176	1.1281	0.8142
(10,10)– (10,10) CNTs	0.1525	1.6732	1.3570
(12, 12)–(12,12) CNTs	0.1674	1.9441	1.6284

In order to dilate CNT macro-structures, in the present work only the transverse extensional force will be considered. This is the key point for the dilatation of CNT fibres and bundles. From Eq. (2), the transversal force (F) per unit length required to reach a relevant deformation is determined as follows

$$F(\delta) = 6.119\frac{|\Phi(d_0)|}{d_0-\rho}\left[\left(\left(\frac{1}{1+0.9179\bar{\delta}}\right)^5 - \left(\frac{1}{1+0.9179\bar{\delta}}\right)^{11}\right)\right] \quad (4)$$

Where δ ($\delta = d - d_o$) is the displacement by the transverse load, and $\bar{\delta} = \delta/(d_0 - \rho)$.

2.2. Dilating CNT membrane using an electrical field

Through this work, a membrane of spinnable Multiwall CNTs (MWCNT) is used, on which some areas are bundles of parallel CNTs and others are very poorly aligned. They entangle together to create a network with an interaction energy as presented in section 2.1. This network entanglement impacts on the elasticity of CNT membrane by slip links (hooks) which can be movable with a constraint imposed by the surrounding CNT fibres. In this research, the energy and then the load to dilate CNT bundles are generated by an electrostatic field. In other words, the electrostatic potential causes the repulsive force between CNT fibres to dilate CNT fibres and bundles.

The experiment is set-up as shown in Figs. 3&4. Voltage applied on the ring electrode using a high voltage amplifier HVA 4321 (NF Corporation) is driven by a function generator 33522A (Keysight Technologies) while CNT membrane is grounded. The waveform is sinusoidal with slew rate of 500V/µs. The width variation of CNT membrane is measured using a high speed camera FASTCAM-1024PCI.

At a relevant voltage, the repulsive force within the charged CNTs is against to the van der Waals between CNT bundles and thus, the CNT membrane is spread. The stretching of CNT membrane depends on the voltage applied on the ring.

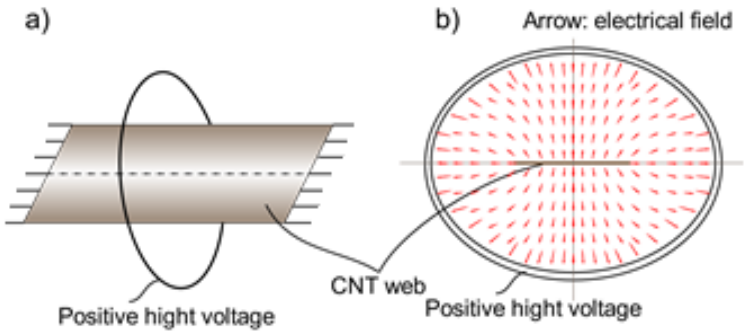

Figure 3 Controlling CNT membrane density using the electrostatic field approach: a) Schematic of the separation of CNT fibres and bundles; and b) A process of the dilatation of CNT fibres and bundles by electrostatic field.

In the present work, a membrane of MWCNTs (1) of 10mm width is pulled out from a wafer of spinnable CNTs (2) grounded (Fig. 4a). A ring of 60mm diameter by steel rod of 2mm diameter is symmetrically installed surrounding the membrane (1) (Fig. 4.b). Under an electric field by different applied voltage, the CNT membrane is enlarged differently as observed in Fig. 5a & b

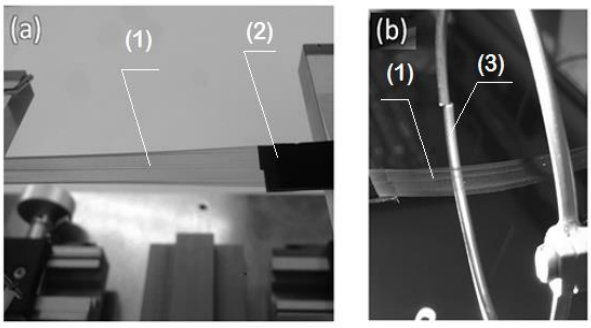

Figure 4. Experiental set-up: (1) CNT membrane; (2) CNT forest; and (3) ring. A range of high voltages is applied on the ring to create electric fields.

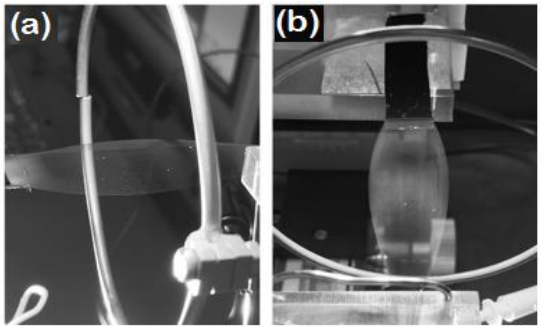

Figure 5. Experimental set-up: Dilatational separation of CNT membranes with different electric fields.

With a range of voltages from 500 V to 5000 V applied on the ring, the electric fields induce a gradual increase of the width of CNT membrane as shown in Fig. 6. The increase of width achieves a stable/maximum value at an applied voltage named as the critical voltage (V_{cr}) whose induced potential and force are greater than the interaction energy between CNTs within the membrane as presented in section 2.1. The interaction energy and then the force depend on the experiment parameters including the CNT membrane density, the relative dielectric coefficient and engineering parameters of ring. For example, in the condition of the present experiment, the width of CNT

membrane reached a stable value of 12 mm, corresponding to an increase of 20% at an applied voltage of 4. kV

At an applied voltage 4kV of the atternating current, a range of frequencies (5, 10, 30 and 100) Hz is used to consider the response of CNT membrance. Results by Fig. 7 show that the lower frequency yields the larger width of CNT membrane. For example, while the width of CNT membrance reaches the biggest increase of 20% with the frequency of 5Hz, this increase is not significant (0.3%) with the frequency of 100 Hz.

In summary, it is worth noting that the higher frequency of AC current yields the higher vibration frequency of membrane, thus, the vibration magnitude decreases as found in Fig. 8. This can be explained as follows: If the specific frequency of the CNT membrane is lower than the frequency of AC current, the frequency of repulsive force by the electrical field is higher than the specific frequency of CNT membrane. In this case, the response of membrane is not enough fast and yields a reduced deformation of membrane. An example of time response of magnitude variation of the CNT membrane using an applied voltage of 4kV and a frequency of 5 Hz is given in Fig. 9.

Based on experimental results by Fig. 8, the present method using AC with very low frequency (5Hz) or direct current was applied to control the density of CNT membranes in several applications mentioned in section 4.

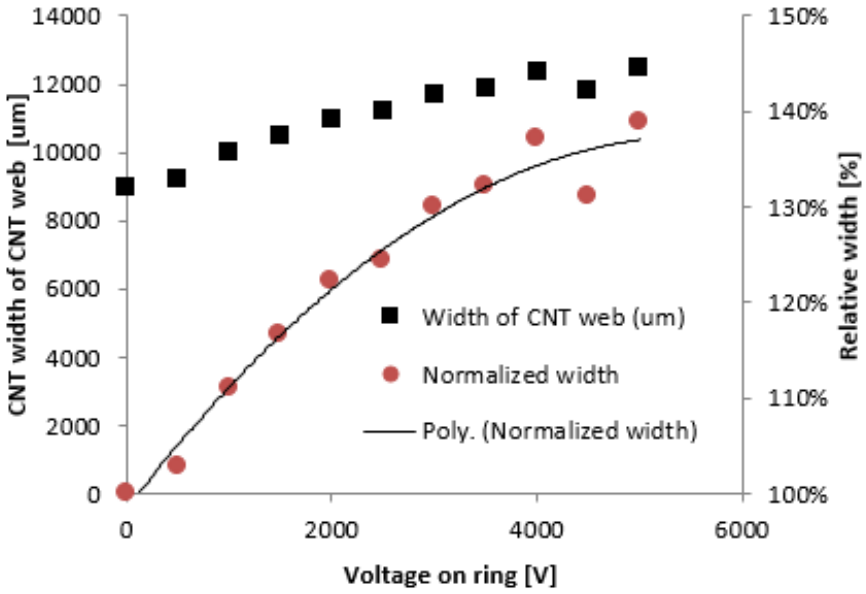

Figure 6. Experimental results: Increment of the width of CNT membrane with a range of the electric field [0kV-5kV]: ■ Width of CNT membrane; ● Normalized width; and ‘continuous line’: the best fitting of normalised width.

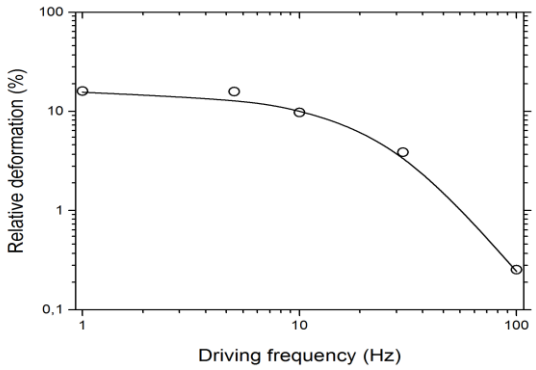

Figure 7: Variation of CNT membrane's width plotted versus the AC frequency using an applied voltage of 4kV

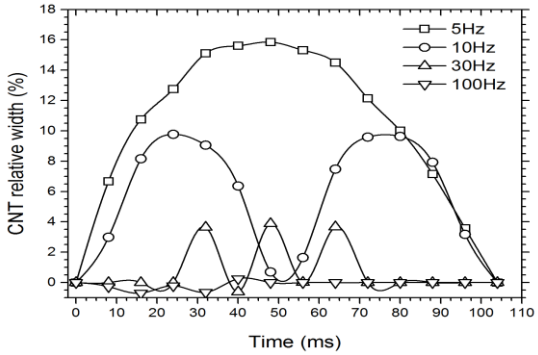

Figure 8: Frequency response with respect to time of CNT membrane width using an applied voltage of 4kV with a range of AC frequencies: 5Hz, 10Hz, 30Hz and 100Hz

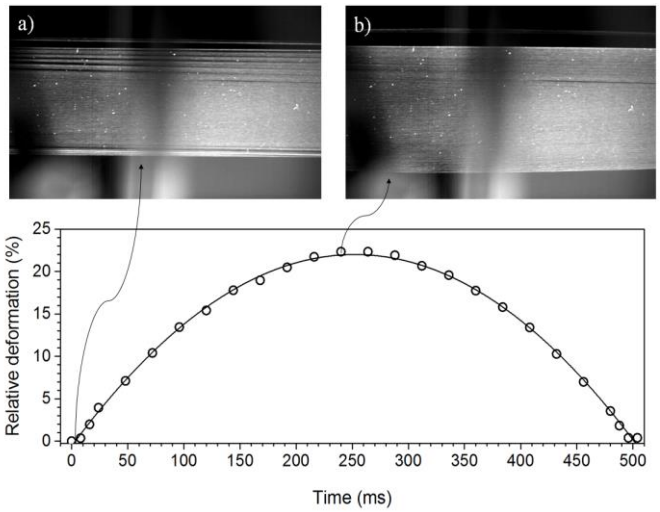

Figure 9 Dilatational separation of CNT membrane using the present method with a frequency of 5Hz and an applied voltage of 4 kV

3. Simulation of the dilatation of CNT membrane using DPD method

A numerical simulation of the present method to enlarge CNT membrane has been carried. This is a multi-physical problem relating to (i) an electrical field generated by a high voltage applied on a ring to create electrostatic force on CNT membrane with residual charges; and (ii) the membrane dilatation caused by the migration of CNT fibers under the electrostatic forces. With a high voltage applied on a ring, the induced electrical potential $\phi(x, y)$is governed by the equation as follows.

$$\nabla \cdot \left(\varepsilon_r \varepsilon_0 \nabla \phi(x,y)\right) = -\rho, \tag{5}$$

where ε_r is the relative dielectric coefficient; ε_0 the vacuum dielectric coefficient (8.854E-12 F/m) and $\rho(\mathrm{x},\mathrm{y})$ the charge density. The electrostatic field is then determined by $\mathrm{E} = -\nabla\phi$.

Assuming that the residual charge density q on the CNT membrane, the Coulomb force given by $F_e = qE$ is introduced into the present system as body force. The dynamic response of a CNT membrane in the electrostatic field is studied using the DPD method where CNT fibers are modelled by a chain of particles whose motion is undergone by the Newton's second law. This approach satisfies conservation laws of mass and momentum and has been applied successfully for several complex-structure fluids including polymer solutions, suspensions of rigid particles, droplets, biological fluids. The CNT membrane with residual charges in CNT networks is set up as shown in Fig. 3

3.1. Dissipative particle dynamics system

In the DPD system, the basic unit consists of a set of discrete momentum carriers called particles/beads that move in continuous space but in discrete time-steps. Particles are acted by three inter-particle forces: the dissipative, random and conservative forces. Hence, each particle moves with their updated velocities for a time-step after a possible collision. The time evolution of each DPD particle (i) governed by Newton's equation of motion for a range of time steps. DPD conserves not only the number of particles but also the total momentum of the system and satisfies Galilean invariance [21].

$$\frac{\mathrm{d}\mathbf{r}_i}{\mathrm{dt}} = \mathbf{v}_i \tag{7}$$

$$m\frac{\mathrm{d}\mathbf{v}_i}{\mathrm{dt}} = \mathbf{f}_i + \mathbf{F}_e \tag{8}$$

where $\mathbf{F}_\mathrm{e}$ is the external force on a particle, and $\mathbf{f}_i$ ($\mathbf{f}_i = \sum_{j\neq i}\left(\mathbf{F}_{ij}^{\mathrm{C}} + \mathbf{F}_{ij}^{\mathrm{D}} + \mathbf{F}_{ij}^{\mathrm{R}}\right)$) the interaction force, consisting of the soft-potential conservative force ($\mathbf{F}_{\mathrm{ij}}^{\mathrm{C}}$), dissipative force ($\mathbf{F}_{\mathrm{ij}}^{\mathrm{D}}$) proportional to the velocity difference, and random force ($\mathbf{F}_{\mathrm{ij}}^{\mathrm{R}}$) modelled by white noise. The random and the dissipative forces are center -to-center and pairwise additive. The interaction forces are given in Table 2.

Table 2. List of interaction forces and weight functions. $\boldsymbol{r}_i$ and $\boldsymbol{v}_i$: the position and velocity of DPD particle *i;* $\boldsymbol{r}_{ij} = \boldsymbol{r}_i - \boldsymbol{r}_j$, $r_{ij} = |\boldsymbol{r}_{ij}|$, $\boldsymbol{v}_{ij} = \boldsymbol{v}_i - \boldsymbol{v}_j$; r_c: the cut off radius; a_{ij}: maximum repulsion between particles i and j; ξ_{ij}: the Gaussian random variable; γ and σ: the amplitude of dissipative and random forces, respectively

$\mathbf{F}_{ij}$	Forms	Weight functions
$\mathbf{F}_{ij}^{C}$	$a_{ij} w^{c} \hat{\boldsymbol{r}}_{ij}$	$w^{C}(r_{ij}) = 1 - r_{ij}/r_c$
$\mathbf{F}_{ij}^{D}$	$-\gamma w^{D}(\hat{\boldsymbol{r}}_{ij} \cdot \boldsymbol{v}_{ij})\hat{\boldsymbol{r}}_{ij}$	$w^{D}(r_{ij}) = (1 - r_{ij}/r_c)^{s}$
$\mathbf{F}_{ij}^{R}$	$\sigma w^{R} \xi_{ij} \hat{\boldsymbol{r}}_{ij}$	$w^{R}(r_{ij}) = \sqrt{w^{D}(r_{ij})}$

3.2. DPD modelling of CNT chains

By connecting DPD particles and spring forces, CNTs can be modelled by the DPD method. The spring model for CNT chains is constructed by linking a series of DPD particles together with spring forces acting between adjacent particles of a CNT as shown in Fig. 10. The force on particle *i* due to particle *j* is given by

$$\mathbf{F}_{ij}^{s} = -\frac{\mathbf{H}\mathbf{r}_{ij}}{\mathbf{1}-\left(\mathbf{r}_{ij}/\mathbf{r}_{m}\right)^{2}} \quad , \tag{9}$$

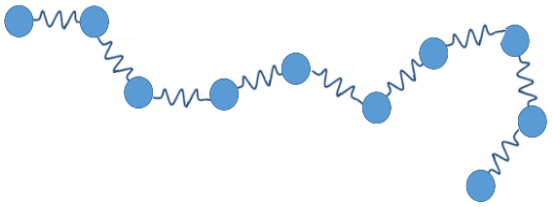

Figure 10. Model of a CNT fiber consisting of several DPD particles connected by springs where H is the spring constant and r_m the maximum length.

van der Waals interactions between the CNTs are represented by simple modifications of the DPD inter-particle forces. The modified version of DPD is developed by introducing a long-range attractive component into the conservative forces. A new conservative particle-particle interaction combining short-range repulsive and long-range attractive interactions to simulate van der Waals interactions. New conservative force between CNT chains $\mathbf{F}_{ij}^{c}$ is calculated by taking derivative with respect to $\boldsymbol{r}$ of a potential like Lennard-Jones potential with attractive and repulsive terms [20].

$$\mathbf{F}_{ij}^{c} = -a_{ij}\left(\mathrm{A}w_r^{c}(r, r_{cr}) - \mathrm{B}w_a^{c}(r, r_{ca})\right)\hat{\boldsymbol{r}}_{ij} \tag{10}$$

where A and B are coefficient of $\boldsymbol{w_r^c(r, r_{cr})}$ and $\boldsymbol{w_a^c(r, r_{ca})}$, respectively; $\boldsymbol{r_{cr}}$ the cut-off radius of repulsive component, $\boldsymbol{r_{ca}}$ radius of attractive component and

$$\mathbf{w_r^c(r, r_{cr})} = \begin{cases} -\mathbf{12}\frac{r}{r_{cr}^2} + \frac{\mathbf{18}r^2}{r_{cr}^3}, & r < \frac{r_{cr}}{2} \\ -\frac{3}{2r_{cr}}\left(\mathbf{2} - \mathbf{2}\frac{r}{r_{cr}}\right)^2, & \frac{r_{cr}}{2} < r < r_{cr} \\ \mathbf{0}, & r > r_{cr} \end{cases}; \quad \mathbf{w_r^c(r, r_{ca})} = \begin{cases} -\mathbf{12}\frac{r}{r_{ca}^2} + \frac{\mathbf{18}r^2}{r_{ca}^3}, & r < \frac{r_{ca}}{2} \\ -\frac{3}{2r_{ca}}\left(\mathbf{2} - \mathbf{2}\frac{r}{r_{ca}}\right)^2, & \frac{r_{ca}}{2} < r < r_{ca} \\ \mathbf{0}, & r > r_{ca} \end{cases}$$

It can be seen by Fig. 11 that the conservative force among different CNT's particles is repulsive (the positive part) when their separation distance is less than the value of radius $\boldsymbol{r}$ (e.g. 0.5952 with $\mathbf{A = 2, B = 1}, \boldsymbol{r_{cr} = 0.8, r_{ca} = 1}$) and when their separation distance falls in the range between 0.5952 and 1, this force describes a long range attraction (the negative part).

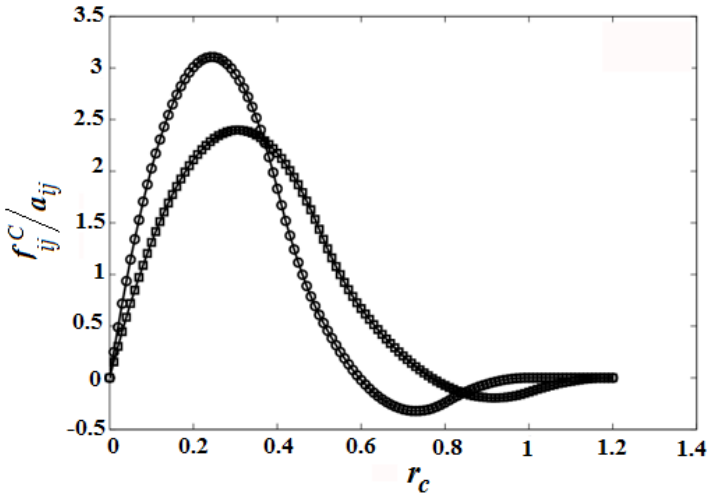

Figure 11: Conservative force with short range repulsion and long range attraction (**–o-**: r_a = 1.0) and (–□– : r_a = 1.2)

3.3. Computational parameters of the problem, results and discussions

A non-dimensional 3D domain of 40 x 9 x 1 (length x width x thickness: unit^3) claimed at two ends as shown in Fig. 12 (also see Fig. 3a). The simulation is performed in the constant number of DPD-CNT beads and constant temperature ensemble. One CNT fibre is considered as a rigid body and modelled as 10 DPD particles linked together by 9 spring chains (Fig. 10). It is worth noting that the balance between dissipative and random forces must satisfy the fluctuation-dissipation theorem [22],[23]. This means that the dissipative parameter (γ) should be proportional to the noise parameter (σ) by $\sigma = \sqrt{2\gamma k_B T}$. It is recommended that σ should be chosen appropriately for maintaining stability of the system, as well as quickly reaching the temperature equilibrium [23]. Thus, the DPD

parameters are determined for the present work as follows: $m_i = 1,\ a_{ij} = 18.75,\ \gamma = \sigma^2 = 4.5,$ $r_{cr} = 0.8, r_{ca} = 1.3$. The density of CNT membrane is 7 DPD particles per a unit cube. A total of 500 chains is generated as depicted in Fig 3.a and Fig. 12a. For the conservative force of DPD, the strengths of repulsive and attractive parts (See Fig. 9) are the value of A = {1} and B = {0.1}, respectively.

Periodic boundary conditions are applied in y-direction meanwhile in x- and z-directions, solid walls are represented by three layers of frozen particles (see Fig. 12a). In the following simulations, the Verlet integration algorithm is employed to solve Eqs. (7) & (8). The simulation is run with 240,000 time steps and a unique time step of 10^{-2} is chosen for all simulations for a range of voltages from 500V to 5000V applied on the ring. Body force caused by the electrical field from the applied voltage on the ring.

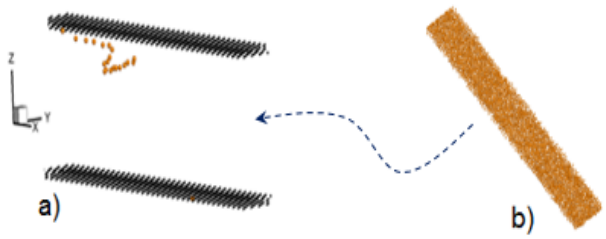

Figure 12. Simulation domain: (a) 3D view of a spring model of a single CNT fibre moving between two walls; and (b) A CNT membrane represented by 500 DPD chains

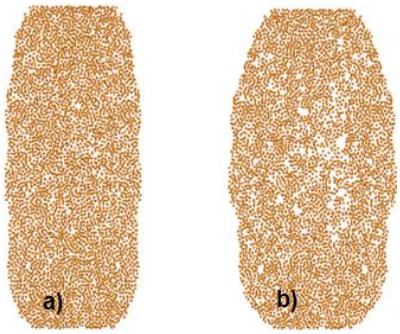

Figure 13. Numerical visualization of the width of CNT membrane increased 120% (a) and 140% (b) with respect to the electric field.

Figure 14 shows the increment of the membrane width with respect to voltages applied on ring (triangles in the figure). These simulated results are in good agreement with those by experiment expressed by red circles. For example, an increase of 120% and 140% for the normalised width of the CNT membrane at the centre of CNT membrane corresponding to 2kV and 5kV respectively as shown in Fig 13. More details and investigations on the simulation using DPD method for processing CNT macrostructures will be presented in our next modelling and simulation work related to this topic.

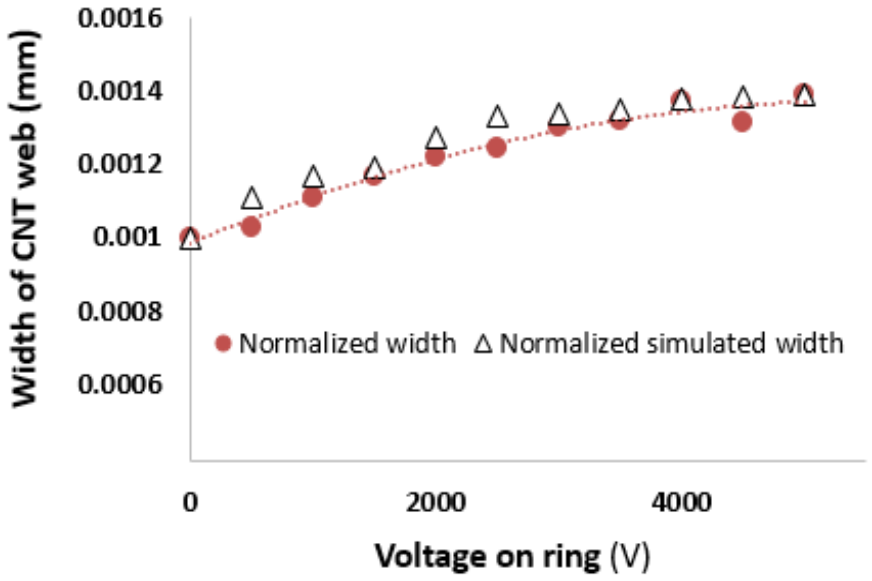

Figure 14. Comparison of the CNT membrane width plotted versus the applied voltage on ring by experiment and the DPD numerical method

4. Several potential applications

The experimental and numerical results are the basis to initially develop several techniques in producing CNT membranes and yarns whose structure can be handled as requested. Such CNT membranes and yarns can be efficiently used as sensors [8], [9], [24]–[26]. The following subsections outline two applications of the present method which have attained some promising results. These applications belong to another research project of us and will be presented with more technique details in our coming papers.

4.1. Multi-step CNT spinning process

Although the recent modified dry spinning process leads to a significant improvement of the properties of a CNT yarn [1], there exists some limits in enhancing the CNTs' alignment in a web because of the fragility of CNT webs while enlarging CNT membranes using mechanical treatment methods. The dilation of membrane using the dielectrophoresis technique allows easily developing a multi-step CNT spinning process (Fig. 15) which further enhances mechanical properties of CNT macrostructures.

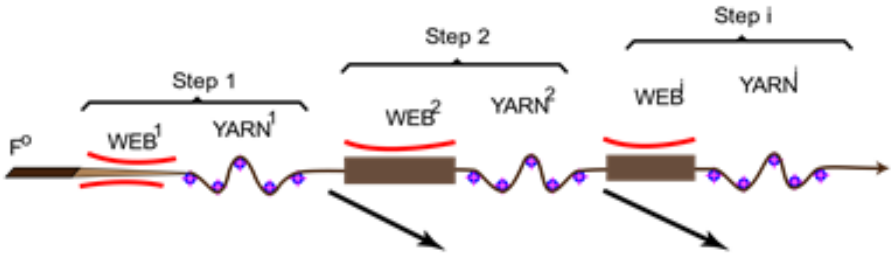

Figure 15 Schematic of the process of multi-step spinning model combined with the dielectrophoresis technique: a) step1: initial CNT web; b) step 2: CNT sliver at the first phase and c) CNT sliver at the second phase. Note: Silver is CNT yarn of low and/or false twist.

With the introduction of the dilatation into the yarn spinning process, the experimental observation found that the alignment of CNTs in a web is gradually improved through the spinning steps and the damage of CNT bundles is significantly reduced [2].

4.2. Manufacturing functional polymer/CNT membranes

A combination between the CNT membrane process using the electric field and polymer nano-fibre electro-spinning technique yields producing functional CNT/polymer macro-structures satisfying various engineering requirements such as absorptive materials and bio-filters where the density of CNTs as well as the porosity of the media can be handled.

Figs. 16 presents the SEM images of several sandwiches of the CNT and polymer fibers by electrospinning technique and CNT membranes treated by the electric field. The multi-layer membranes produced by the present scheme can satisfy requirements on the mechanical and physical properties including the porosity, tenacity and absorbability.

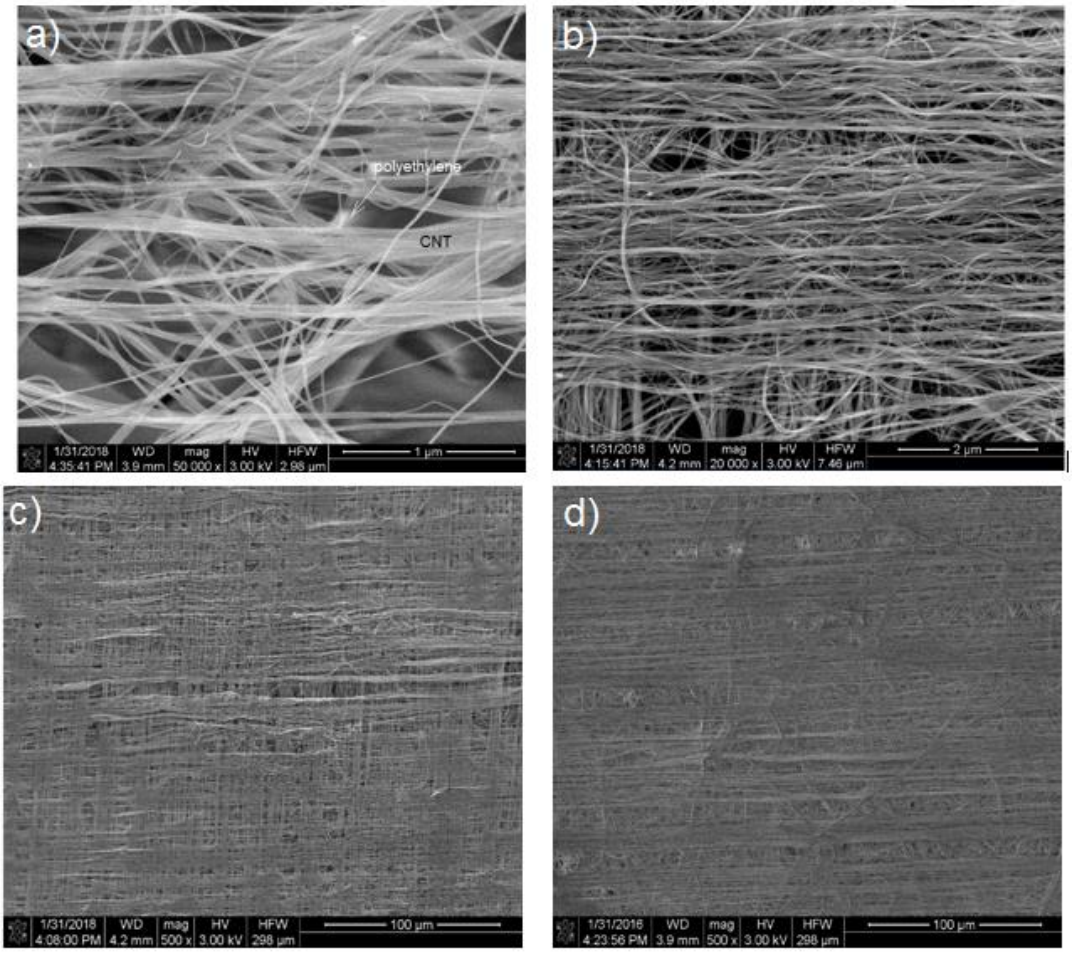

Figure 16 SEM images of functional multi-layer macrostructures using poly-urethane nano-fibers spayed on CNT membrane of two directions with different magnifications: (a) sample with magnification of 50000; (b) sample with magnification of 20000 and (c)&(d) two different samples with magnification of 500.

5. Conclusion

This paper reports an approach to process CNT membranes using the dielectrophoresis method, in which CNT fibres and/or bundles are dilated in webs as well as in CNTs based macrostructures. This helps partially eliminate the agglomeration of CNTs and other nano-particles into in several different processing. The present approach, based on the slip-link entanglement model and the electric field to separate CNTs from each other, yields a new technique to control the density/porosity which affects physical and mechanical properties of CNT macrostructures. Experimental results of the present method have been successfully simulated using the DPD method. Finally, several potential applications of the method have also been devised.

Acknowledgements

The first author would like to thank Professor Nhan Phan-Thien, Department of Mechanical Engineering, National University of Singapore for his great support on the research fellowship in the framework of ADOSP by the University of Southern Queensland in 2017.

Reference

[1] C. D. Tran, W. Humphries, S. M. Smith, C. Huynh, and S. Lucas, "Improving the tensile strength of carbon nanotube spun yarns using a modified spinning process," *Carbon N. Y.*, vol. 47, no. 11, pp. 2662–2670, 2009.

[2] C.-D. Tran, "Dry Spinning Carbon Nanotubes into Continuous Yarn: Progress, Processing and Applications," in *Nanotube Superfiber Materials Changing Engineering Design*, 2014, p. 211.

[3] C. D. Tran, S. Lucas, D. G. Phillips, L. K. Randeniya, R. H. Baughman, and T. Tran-Cong, "Manufacturing polymer/carbon nanotube composite using a novel direct process," *Nanotechnology*, vol. 22, no. 14, p. 145302, 2011.

[4] A. A. Kuznetsov, A. F. Fonseca, R. H. Baughman, and A. A. Zakhidov, "Structural model for dry-drawing of sheets and yarns from carbon nanotube forests," *ACS Nano*, vol. 5, no. 2, pp. 985–993, 2011.

[5] X. Zhang *et al.*, "Spinning and processing continuous yarns from 4-inch wafer scale super-aligned carbon nanotube arrays," *Adv. Mater.*, vol. 18, no. 12, pp. 1505–1510, 2006.

[6] J. J. Vilatela, J. A. Elliott, and A. H. Windle, "A model for the strength of yarn-like carbon nanotube fibers," *ACS Nano*, vol. 5, no. 3, pp. 1921–1927, 2011.

[7] M. Doi and J. Takimoto, "Molecular modelling of entanglement.," *Philos. Trans. A. Math. Phys. Eng. Sci.*, vol. 361, no. 1805, pp. 641–652, 2003.

[8] T. Dinh *et al.*, "Environment-friendly carbon nanotube based flexible electronics for noninvasive and wearable healthcare," *J. Mater. Chem. C*, vol. 4, no. 42, 2016.

[9] T. Dinh *et al.*, "Polyacrylonitrile-carbon Nanotube-polyacrylonitrile: A Versatile Robust Platform for Flexible Multifunctional Electronic Devices in Medical Applications," *Macromol. Mater. Eng.*, vol. 5, pp. 19000141–8, 2019.

[10] M. Senthil Kumar *et al.*, "DC electric field assisted alignment of carbon nanotubes on metal electrodes," *Solid. State. Electron.*, vol. 47, no. 11, pp. 2075–2080, 2003.

[11] B. H. Fishbine, "Carbon nanotube alignment and manipulation using electrostatic fields," *Fuller. Sci. Technol.*, vol. 4, no. 1, pp. 87–100, 1996.

[12] A. Ural, Y. Li, and H. Dai, “Electric-field-aligned growth of single-walled carbon nanotubes on surfaces,” *Appl. Phys. Lett.*, vol. 81, no. 18, pp. 3464–3466, 2002.

[13] A. Nojeh, A. Ural, R. F. Pease, and H. Dai, “Electric-field-directed growth of carbon nanotubes in two dimensions,” *J. Vac. Sci. Technol. B Microelectron. Nanom. Struct.*, vol. 22, no. 6, p. 3421, 2004.

[14] C.-D. Tran, T. Tran-cong, K. Le-Cao, and D. Ho-Minh, “Processing the CNTs ’ interaction in web using an electrostatic field based process,” in *the International Conference on Nanoscience and Nanotechnology (ICONN 2012)*, 2012, pp. 233–234.

[15] H.A. Pohl, *Dielectrophoresis: The Behavior of Neutral in Nonuniform Electric Fields*. Cambridge: Cambridge University Press, 1978.

[16] D. W. Coffin, L. A. Carlsson, and R. B. Pipes, “On the separation of carbon nanotubes,” *Compos. Sci. Technol.*, vol. 66, no. 9, pp. 1129–1137, 2006.

[17] L. A. Girifalco, M. Hodak, and R. S. Lee, “Carbon nanotubes, buckyballs, ropes, and a universal graphitic potential,” *Phys. Rev. B - Condens. Matter Mater. Phys.*, vol. 62, no. 19, pp. 13104–13110, 2000.

[18] L. A. Girifalco and R. A. Lad, “Energy of Cohesion, Compressibility, and the Potential Energy Functions of the Graphite System,” *The Journal of Chemical Physics*, vol. 25, no. 4. pp. 693–697, 1956.

[19] L. A. Girifalco, M. Hodak, and R. S. Lee, “Carbon nanotubes, buckyballs, ropes, and a universal graphitic potential,” *Physical Review B - Condensed Matter and Materials Physics*, vol. 62, no. 19. pp. 13104–13110, 2000.

[20] M. Liu, P. Meakin, and H. Huang, “Dissipative particle dynamics simulation of multiphase fluid flow in microchannels and microchannel networks,” *Phys. Fluids*, vol. 19, p. 033302, 2007.

[21] C. A. Marsh, “Theoretical Aspects of Dissipative Particle Dynamics,” 1998.

[22] A. G. Schlijper, P. J. Hoogerbrugge, and C. W. Mamke, “Computer simulation of dilute polymer solutions with the dissipative particle dynamics method,” *J. Rheol. (N. Y. N. Y).*, vol. 39, pp. 567–579, 1995.

[23] R. D. Groot and P. B. Warren, “Dissipative Particle Dynamics: Bridging the Gap between Atomistic and Mesoscopic Simulation,” *J. Chem. Phys.*, vol. 107, no. 11, p. 4423, 1997.

[24] T.-K. Nguyen *et al.*, “Electrically Stable Carbon Nanotube Yarn under Tensile Strain,” *IEEE Electron Device Lett.*, vol. 38, no. 9, 2017.

[25] T. Dinh *et al.*, “Electrical resistance of carbon nanotube yarns under compressive transverse pressure,” *IEEE Electron Device Lett.*, vol. 39, no. 4, pp. 584–587, 2018.

[26] T. Dinh, T. K. Nguyen, H. P. Phan, C. D. Tran, and V. Dau, “Carbon nanotube four-terminal devices for pressure sensing applications,” in *Smart Innovation, Systems and Technologies*, S. R. Vlacic L., Dao D., Howlett R.J., Ed. Springer, 2019, pp. 199–207.